Applied Materials Today 25 (2021) 101236

Contents lists available at ScienceDirect

Applied Materials Today

journal homepage: www.elsevier.com/locate/apmt

Spatially selective adhesion enabled transfer printing of liquid metal for 3D electronic circuits

Rui Guo[a], Yang Zhen[b], Xian Huang[b], Jing Liu[a,c,*]

[a] Department of Biomedical Engineering, School of Medicine, Tsinghua University, Beijing, China
[b] Department of Biomedical Engineering, Tianjin University, Tianjin, China
[c] Beijing Key Lab of CryoBiomedical Engineering and Key Lab of Cryogenics Technical Institute of Physics and Chemistry, Chinese Academy of Sciences, Beijing 100190, China

ARTICLE INFO

Article history:
Received 6 September 2021
Revised 10 October 2021
Accepted 19 October 2021
Available online 28 October 2021

Keywords:
Liquid metal
Selective adhesion
Transfer printing
3D electronic circuits

ABSTRACT

3D printing, well known by the public, is regarded as an important symbol of entering the next industrial revolution that is well suited for the development of 3D electronics. However, reducing the manufacturing cost and time of 3D electronics is still one of the biggest challenges for its wide application. With low melting point, high conductivity, and reversible stiffness, gallium-based liquid metals are of great importance in developing multifunctional 3D electronic circuits. While, most research only use liquid metal as filler in 3D channels, which greatly weakened the interface function of liquid metal. Here, we report a straightforward, practical, and rapid fabrication strategy for multifunctional 3D electronic circuits based on 3D printing and a spatially selective adhesion mechanism of liquid metal inks. This method is applicable to diverse 3D structures with various mechanical properties and material types. A series of electronic circuits were printed out, and conceptual experiments were performed to demonstrate and justify the working of the new approach. Because of the phase transition and contact welding, the liquid metal based 3D electronic circuits show excellent stiffness variation and assemblability, which are promising to fabricate complex flexible 3D electronic systems, reconfigurable 4D electronics, and variable stiffness robots.

1. Introduction

With the potential for new characteristics and functionalities on complex 3D surface, 3D electronics have been increasingly evaluated for many applications, such as wearable electronics, implantable devices, reconfigurable electronics, conformal antennas and artificial skin for smart robots. [1–4] While, most electronics are printed on planar rigid or flexible substrates using microfabrication based on lithography, etching, inkjet and transfer printing, which are still not idealistically compatible with complex 3D substrates. At present, three-dimensional printing has been widely employed in the world as a relatively matured technology, which can access any complex structure in principle. However, it is limited that most 3D printed materials are non-conductive. Although metal 3D printing has achieved many results, the high manufacturing costs seriously limits its wide application in consumer electronics. [5] Therefore, improved 3D printing methods are important way in fabricating 3D electronics, such as multiprocess sequential writing, [6] direct writing, [7, 8] laser writing, [9] charge-programmed 3D printing. [10] Additional printing steps lead to excessive printing time, and the difficulty of printing path optimization will increase significantly with the complexity of the 3D structures. As an alternative, more 3D electronics are realized by transfer printing [11–13] or mechanical assembly [14, 15] the planar electronic devices onto 3D surface. However, the classical transfer printed planar electronics require matched bendability, stretchability, and conformability with 3D substrates, and the mechanical assembly requires complicated structure design optimization, which increase their preparation cost and time. Besides, the approach of depositing conductive coatings on traditional materials shows great promise in the reduction of preparation cost and time. [16] Current, the electrochemical reaction still requires a long time and the reaction solution requires high preparation cost.

Recently, with high conductivity, compliance and low toxicity, gallium-based liquid metals have recently received considerable attention for wide applications in flexible electronics, [17] soft robots, [18] and biomedical devices. [19, 20] Nowadays, most preparation methods of liquid metal electronics are still somewhat confined to planar structures, and the current 3D liquid metal electronics preparation methods are only improvement of the pla-

* Corresponding author.
E-mail address: jliubme@tsinghua.edu.cn (J. Liu).

https://doi.org/10.1016/j.apmt.2021.101236
2352-9407/

nar liquid metal electronics, such as microchannel injection, [21–23] coaxial nozzle-printing, [24, 25] direct writing [26–31] and transfer printing. [32, 33] With low melting point, the liquid metals have obvious stiffness variation through changes in temperature, which are able to provide more functions for 3D electronics as phase-changing material. [34–37]

Here, we introduced a fast transfer printing method to produce liquid metal 3D electronic circuits by realizing liquid metal conductive coating on the surface of 3D structures. The method was based on controlling the selective adhesion of liquid metal between 3D substrate materials and adhesive coating. With this approach, we demonstrated various complex 3D electronics using common commercial 3D printing technologies, which displayed the advantages of simple, fast and low cost. Furthermore, the liquid metal coating showed some special functions of low melting point alloys. For example, liquid bridge enabled low temperature welding made it possible to assemble complex reconfigurable 3D or 4D electronics. The phase transformation of liquid metal coating was demonstrated as spatial stiffness adjustable exoskeleton for a robot. In addition to 3D printing materials, the present technique, combined with multifunctional materials, allowed 3D electronics with diverse mechanical properties, such as stretchable electronics and lightweight electronics.

2. Experimental section

2.1. Materials

Gallium and indium (Anhui Minor New Materials Co. Ltd., 99.999% purity) were used as the metallic liquid base. The gallium-indium eutectic alloys (EGaIn, 75.5 wt% gallium and 24.5 wt% indium with melting point of 15 °C and electrical conductivity of 3.4×10^6 S m^{-1}) was prepared by heating and mixing gallium and indium together at 160 °C for 30 min. The previous studies had shown that the EGaIn was easily oxidized in air, and there was a metal oxide layer covered on the EGaIn surface. Here, O-EGaIn was obtained by scraping the metal oxide layer covered on the EGaIn surface by a scraper. Then, the scraped O-EGaIn was collected together. In order to obtain O-EGaIn with the same oxidation, the scraping operation was carried out at room temperature. Besides, the depth of the scraper inserted into the liquid metal will affect the content of liquid metal oxides in the O-EGaIn. The deeper the scraper is inserted into the liquid metal, the more liquid metal it carried, which will reduce the content of metal oxides. Therefore, the scraper only needs to touch the liquid metal surface slightly, as shown in Figure S2b. The polymethacrylates (PMA) glue was purchased from Hong Kong Yihui Co. Ltd. The 3D stretchable soft structures were prepared by perfusion molding process using Ecoflex 00–30 (Smooth-On, PA, USA), which was prepared by mixing two precursor materials at weight ratio of 1:1 and cured at room temperature for 4 h.

2.2. Printing methods of printed structures

In this research, three 3D printing methods were used to construct 3D structures of various materials. First, a 3D printing machine (Fuse1, Deed3D Technology Co., Ltd, Guangzhou, China) was used to print structures of nylon (polyamide, PA) and fiberglass reinforced nylon with a printing resolution of 200 μm based upon the selective laser sintering (SLS) technique. Second, a 3D printing machine (HP Jet Fusion 4200, HP Development Company, L.P. USA) was used to print structures of nylon with a printing resolution of 200 μm based upon the multi jet fusion (MJF) technique. Finally, a 3D printing machine (CL-60 HALOT-1, Creality 3D Technology Co., Ltd, Shenzhen, China) was adopted to print structures of photopolymer with a printing resolution of 50 μm based upon the sereolithography apearance (SLA) technique.

2.3. Chemical composition and mechanical property characterization

The energy-dispersive X-ray spectrum (EDS, GENESIS, America) was used to identify the distribution of elements (Ga, In and O) on the EGaIn and O-EGaIn surface. The impacting behaviors of the EGaIn and O-EGaIn were investigated to demonstrate the lower fluidity of O-EGaIn. Here, the EGaIn and O-EGaIn droplets were dropped on a glass plate from 0.5 m above, and a high-speed camera (IDT NR4 S3 high-speed data acquisition instrument) was used to record the sequential images during the impact process of droplets. A dynamic mechanical analysis test was carried out on the TST350 system with LNP95.

2.4. Surface and adhesion characterization

The microscopic images of various 3D structures and PMA glue were captured with scanning electron microscopes (S-4300, Japan). The confocal laser scanning microscope (VK-X250, Japan) was used to measure the surface 3D topography of various 3D structures, printed PMA glue and O-EGaIn lines covered on 3D substrates. The contact angle meter (XG-CAMC) was used to measure the contact angle of the O-EGaIn droplets on 3D structure with photopolymer and printed PMA glue. The adhesive force of 3D structure with photopolymer and printed PMA glue with O-EGaIn was measured by a dynamic contact angle measurement system (DCAT 11, DataPhysics Instruments GmbH). Here, a 3D printed round rod with photopolymer (cross-sectional radius: 2 mm, length: 50 mm) which is connected to a fixed stress sensor was first pushed into the O-EGaIn (inserting depth of 2 mm) and then pulled out at a controlled speed (0.05 mm s^{-1}). The force acting on the round rod was recorded during the whole process. The maximal tension on the round rod was the adhesive force. Later, PMA glue was printed on the surface of this round rod, and repeat the above operation.

2.5. Electrical performance measurement

The resistance of O-EGaIn lines printed on 3D structures was measured using a digital multimeter (Agilent 34,420). The frequency-dependent measured reflection coefficients of the 3D antenna based O-EGaIn was measured by the vector network analyzer (Hewlett-Packard 8753D). The strain−resistance curve of 3D mesh line based on O-EGaIn was measured with a universal testing machine (Shimadzu, Model AGS-X) and a digital source meter (Keithley, Model 2400).

3. Results and discussion

The present fabrication scheme of liquid metal 3D circuits is based on the selective adhesion mechanism of oxidized liquid metal between 3D-printed substrate materials and the adhesive coating. Due to high surface tension and solid oxide layer covered on the surface, it is generally difficult for gallium-based liquid metal (EGaIn) to be adhered to many 3D-printed substrate materials. In order to improve the adhesion of liquid metal on 3D structures, a kind of adhesive coating, polymethacrylates (PMA) glue, is pre coated on the surface of 3D structures. Besides, with excellent mobility, EGaIn can easily flow away from the surface of 3D structures under the action of gravity, Hence, we use oxidized liquid metal (O-EGaIn) with poor fluidity as the conductive coating for 3D circuits. A brief illustration of the fabrication scheme is shown in Fig. 1a. A 3D-printed structure was directly soaked in PMA glue for 10 s. At room temperature, the 3D structure with PMA coating

Fig. 1.. The fabrication scheme of liquid metal 3D circuits. (a) Brief illustration of the whole process of 3D transfer printing. (b) Selective laser sintering (SLS), multi jet fusion (MJF), and sereolithography apearance (SLA) are utilized to fabricate 3D structures; Nylon (polyamide, PA), fiberglass reinforced nylon and photopolymer are selected as 3D-printed substrate materials. (c) Photographs of a series of complex 3D conductive structures fabricated by liquid metal 3D transfer printing.

was placed in the air until the PMA coating solidified into membrane. Then, the 3D structure with PMA coating was slowly inserted into O-EGaIn. Finally, the 3D structure was smoothly pulled out of O-EGaIn. Due to the high adhesive of PMA coating, the O-EGaIn was uniformly adhered to the surface of 3D structure Video S1 demonstrates the process of O-EGaIn based 3D transfer printing method, which is completed within a few minutes. To inspect the performance of different 3D printing techniques for O-EGaIn based 3D circuits, we adopted three of the most commonly used 3D printing methods, such as selective laser sintering (SLS), multi jet fusion (MJF), and sereolithography apearance (SLA), to fabricate 3D structures (see Methods). Meanwhile, we adopted three kinds of 3D-printed substrate materials, such as nylon (polyamide, PA), fiberglass reinforced nylon and photopolymer to demonstrate the broad applicability of O-EGaIn based 3D transfer printing method. As shown in Fig. 1b and Figure S1, the PMA coating can be formed on the four kinds of 3D-printed structures, and the O-EGaIn coating also can be adhered to the surface of these 3D structures. Furthermore, thanks to the advantage of 3D printing technology in manufacturing complex structures, a series of complex 3D conductive structures could be formed (Fig. 1c and Video S2).

Fig. 2a shows the preparation method of O-EGaIn, which was scraped from the surface of EGaIn (Figure S2 and Video S3). The photographs of EGaIn and O-EGaIn show that there were more metal oxides covering the surface of EGaIn. The previous researches have established that EGaIn adheres to substrates mainly due to the formation of oxide layer on the surface, and the solid metal oxides (Ga_2O_3) will reduce the surface tension and mobility of EGaIn. [38] Consequently, there was no offset of position under the influence of gravity for the O-EGaIn adhered to a vertical plane, while the EGaIn flowed away from the vertical plane, as shown in Fig. 2b. Because of the existence of excessive metal oxides, O-EGaIn was in the semiliquid state, which had fluidity and rigidity (identify liquid and solid, respectively). Therefore, impacting tests were adopted to characterize the semiliquid state features of O-EGaIn compared with EGaIn. As shown in Fig. 2c, EGaIn revealed a liquid-like impact on the behaviors, which had a longer impacting duration (3 ms) and higher expanding ratio of the droplet rim d_x/d_0 (6.33), while O-EGaIn showed a clear indication of rigidity increase. Its impacting duration was only about 2 ms, and expanding ratio of the droplet rim d_x/d_0 was about 2.14. In order to explain the difference of mechanical properties between EGaIn and O-EGaIn,

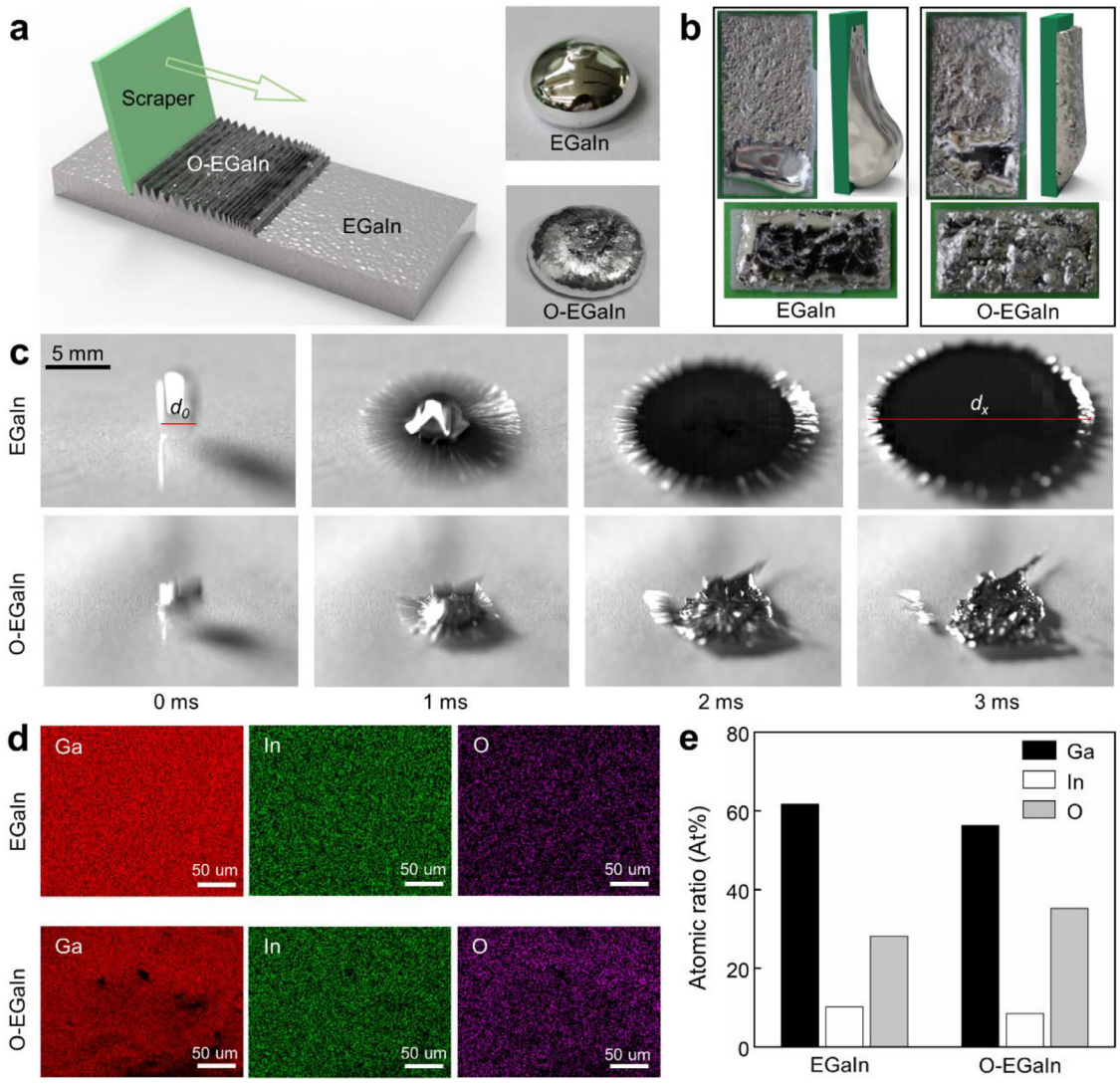

Fig. 2.. Mechanical property and chemical composition characterization of EGaIn and O-EGaIn. (a) The preparation method of O-EGaIn. (b) Diagrams and photos about the influence of gravity for O-EGaIn and EGaIn. (c) The sequential images during the impact process of EGaIn and O-EGaIn droplets. (d) Element distribution mapped by EDS of EGaIn and O-EGaIn. (d) The atomic ratio of Ca, In and O on the surface of EGaIn and O-EGaIn.

further inspections on the chemical compositions of EGaIn and O-EGaIn was made by EDS. Maps of element distribution in Fig. 2d shows the existence of Ga, In and O on the surface of EGaIn and O-EGaIn. Meanwhile, as can be seen from the maps of oxygen element distribution, there is more oxygen distributing on the surface of O-EGaIn. Fig. 2e quantitatively shows the atomic ratio of Ga, In, and O on the surface of EGaIn and O-EGaIn. It is obvious that the atomic ratio of O on the surface of O-EGaIn (35.2%) is higher than that of EGaIn (28.1%).

In this research, we found that the selective adhesion of O-EGaIn between 3D substrate materials and PMA coating was significant. Here, three experiments were carried out to demonstrate the outstanding adhesive selection of O-EGaIn on the surface of the PMA coating than the 3D substrates. In order to simplify the experimental method, we only used SLA printed photopolymer as the 3D substrate. At first, the adhesion changes of 3D substrates before and after printing the PMA coating were studied by contact angle measurement. As shown in Fig. 3a, the contact angle of O-EGaIn droplets on the 3D substrate was about 140°, while on the PMA coating it was about 64° According to the classical definition of wettability of liquid on solid surface, the wettability of liquid on solid surface decreases with increased contact angles. Thus, the wettability of O-EGaIn droplets on PMA coating was apparently higher than that on 3D substrate. Then, a push-pull method was introduced to characterize the adhesive force of O-EGaIn on the 3D substrate and the PMA coating (Figure S3). Fig. 3b presents the F-Position curves of O-EGaIn on the 3D substrate and the PMA coating during the push-pull test. It could be seen that the maximal force (5.4 mN) on the probe covered with the PMA coating was much larger than that on the 3D substrate (1.9 mN). Finally, we printed PMA to different positions of the 3D printed rod using a brush, as shown in Fig. 3c. After inserting these round rods into O-EGaIn and taking them out, we found that the O-EGaIn adhered only to areas coated with PMA (Video S4). Besides, the microscopic images obtained by the contact angle meter in Figure S4 show that there is about 66 μm thick O-EGaIn adhered to the surface of 3D printed round rods.

A series of conceptual experiments have also been conducted to reveal more detailed information on how the PMA coating impacted interfacial properties of 3D substrate materials and O-EGaIn system. PMA was first printed on four kinds of 3D substrates, including SLA printed photopolymer, MJF printed nylon, SLS printed nylon, and fiberglass reinforced nylon (Figure S5). SEM images in Fig. 3d show the surface morphology of these substrates before

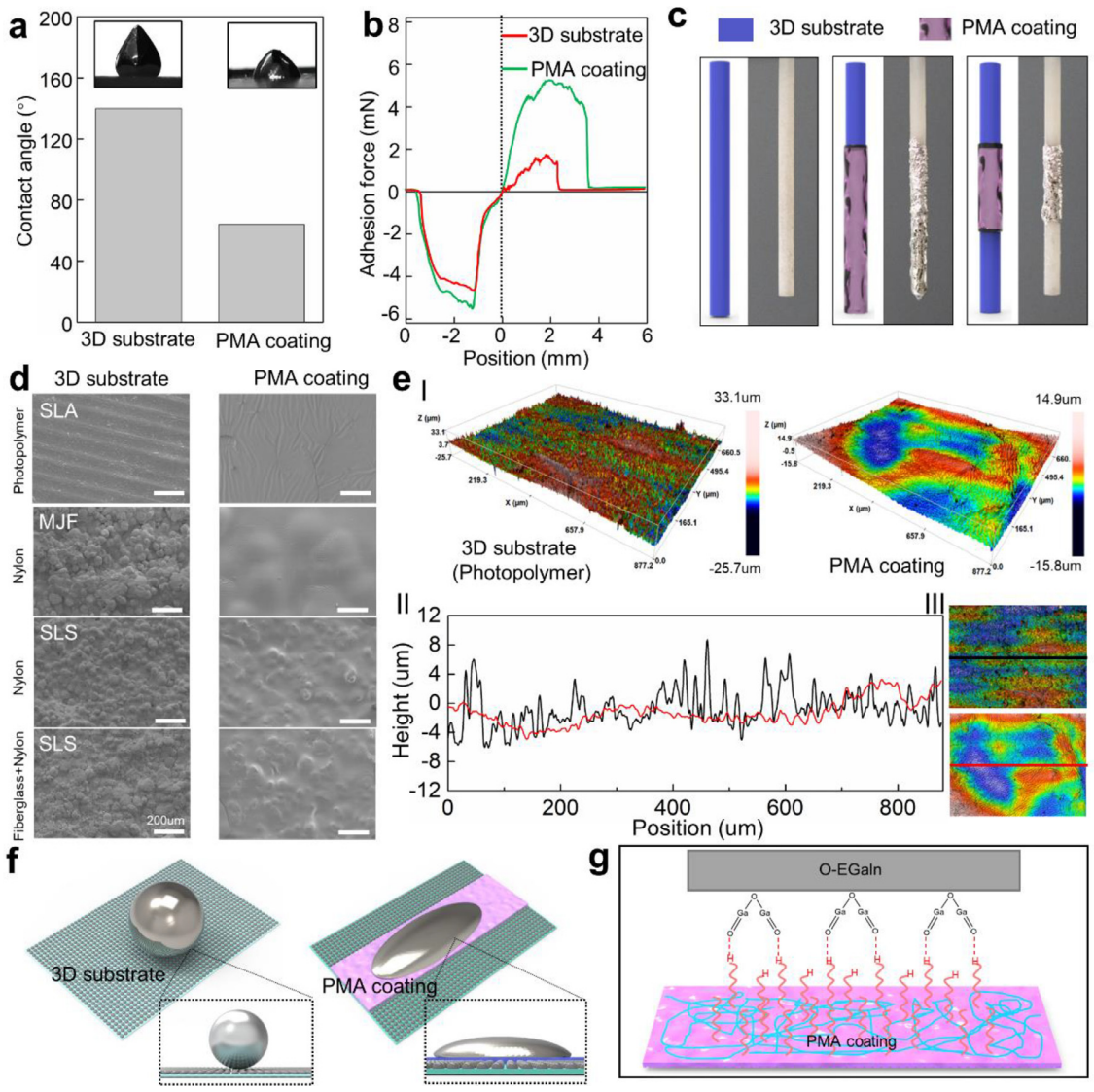

Fig. 3.. Surface and adhesion characterization of 3D substrate and PMA coating. (a) The contact angle of O-EGaIn droplets on 3D substrate and PMA coating. (b) The F-Position curves of O-EGaIn on 3D substrate and PMA coating during the push- pull test. (c) PMA glue was printed to different positions of the 3D printed rod using a brush and the O-EGaIn adhered only to target areas coated with PMA glue. (d) SEM images of four kinds of 3D substrate samples before and after printing PMA glue. (e)I 3D surface profile structures of SLA printed photopolymer and PMA coating. (e)II Two profile curves at the center of 3D surface profile of 3D substrate (black line) and PMA coating (red line). (e)III The position of two profile curves curve in the 3D surface profile structures. (f) Schematic illustration of the effect of surface roughness on O-EGaIn adhesion. (g) Schematic illustration of the hydrogen bonds between O-EGaIn and PMA coating.

and after printing PMA. As observed from the results in Fig. 3d, the surface roughness of these 3D substrates has been significantly reduced, as the voids on the surface of these substrates have been filled with PMA. However, the surfaces of SLS printed nylon and fiberglass reinforced nylon substrates are too rough to form a smooth and flat PMA coating. Besides, the 3D surface profile structures of SLA printed photopolymer measured by a confocal laser scanning microscope in Fig. 3eI manifested that the 3D substrate surface had obvious rough micro particle structures. In order to quantitatively describe the surface roughness of the 3D substrates and PMA coating, we selected two profile curves (Fig. 3eII) at the center of 3D surface profile of 3D substrate (black line in Fig. 3eIII) and PMA coating (red line in Fig. 3eIII), respectively. The arithmetic average deviation value (R_a) were calculated according to Equation 1.

$$R_a = \frac{1}{L}\int_0^L |y|dx \quad (1)$$

where, the L is measuring length of surface, the y is distance from each point on the contour to the centerline. The R_a of 3D substrate is about 2.24 um, and that of PMA coating is about 1.35 um. Figure S6–8 show the 3D surface profile structures and profile curves of MJF printed nylon (black line: R_a= 20.88 um; red line: R_a= 15.68 um), SLS printed nylon (black line: R_a= 12.74 um; red line: R_a= 9.00 um) and fiberglass reinforced nylon (black line: R_a= 13.82 um; red line: R_a= 10.02 um), respectively.

In summary, the structures made by common 3D printing technology have micro rough surfaces, which can attract air effectively in the gaps and decrease the effective contact area between O-EGaIn and 3D structures. [41] Thus, O-EGaIn can hardly adhere to the surface of 3D structures. However, PMA coating can be filled into the tiny gaps, and form smooth surface, which increases the effective contact area, as shown in Fig. 3f. Besides, previous studies noted that there was a large quantity of hydroxyl group in PMA coating, which could form strong hydrogen bond with the oxide layer of O-EGaIn, [40] as shown in Fig. 3g. Therefore, under the

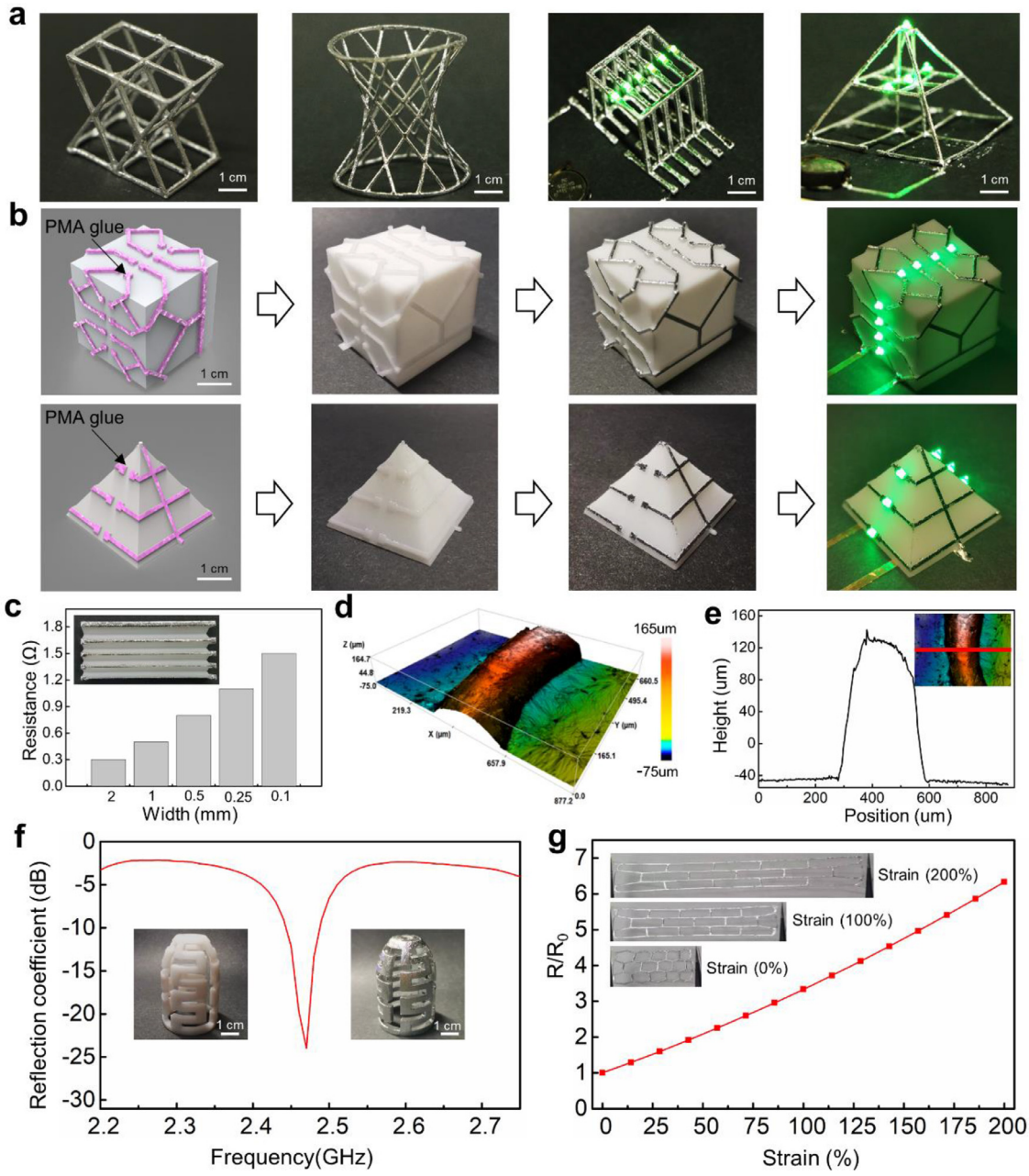

Fig. 4.. Electrical performance of O-EGaIn 3D electronics. (a) Complex 3D mesh structures completely covered O-EGaIn were used to connect electronic components. (b) The preparation of O-EGaIn electronics on the surface of a cube and square pyramid. (c) The resistance of different width of O-EGaIn wires on a 3D structure. (d) The 3D surface profile structure of an O-EGaIn wire. (e) The profile curve at the center of 3D surface profile. (f) The frequency-dependent measured reflection coefficients of the 3D antenna. (g) The relative resistance curve of the 3D mesh electronic under various strains.

synergistic influence of surface morphology and hydrogen bond, O-EGaIn was selectively adhered to PMA coating instead of 3D substrates.

The O-EGaIn covering the 3D structure made it possible to one-step fabricate complex 3D electronic. Here, all the 3D printed structures were fabricated using SLA printed photopolymer. As shown in Fig. 4a, reticular 3D structures covered O-EGaIn were similar to the conducting wires, which could be used to connect electronic components in 3D circuits. Besides, PMA glue could be applied only to specific parts of the 3D structures to fabricate more complex electronics on the surface of 3D structures. Fig. 4b shows the preparation of O-EGaIn electronics on the surface of a cube and square pyramid, where the O-EGaIn was adhered to specific parts to connect LED lights. To assess the electrical performance of the O-EGaIn wires on the surface of 3D structures, the resistance of different width of O-EGaIn wires (length of 5 cm) on a 3D structure was characterized, as shown in Fig. 4c. The resistance of O-EGaIn wires increased gradually with the decrease of the lines width. While, there was nonlinear relationship between resistance of O-EGaIn wires and their width. Thus, the 3D surface profile structure of an O-EGaIn wire was measured by a confocal laser scanning microscope (Fig. 4d). The profile curve in Fig. 4e was selected at the center of 3D surface profile (red line). It could be seen that the cross-sectional morphology was uneven. In addition to being used as a conductor for connecting electronic components, O-EGaIn electronics itself could be served as functional devices with complex 3D structures. Here, we designed a 3D antenna with a reflection coefficient of −24 dB at 2.47 GHz by completely

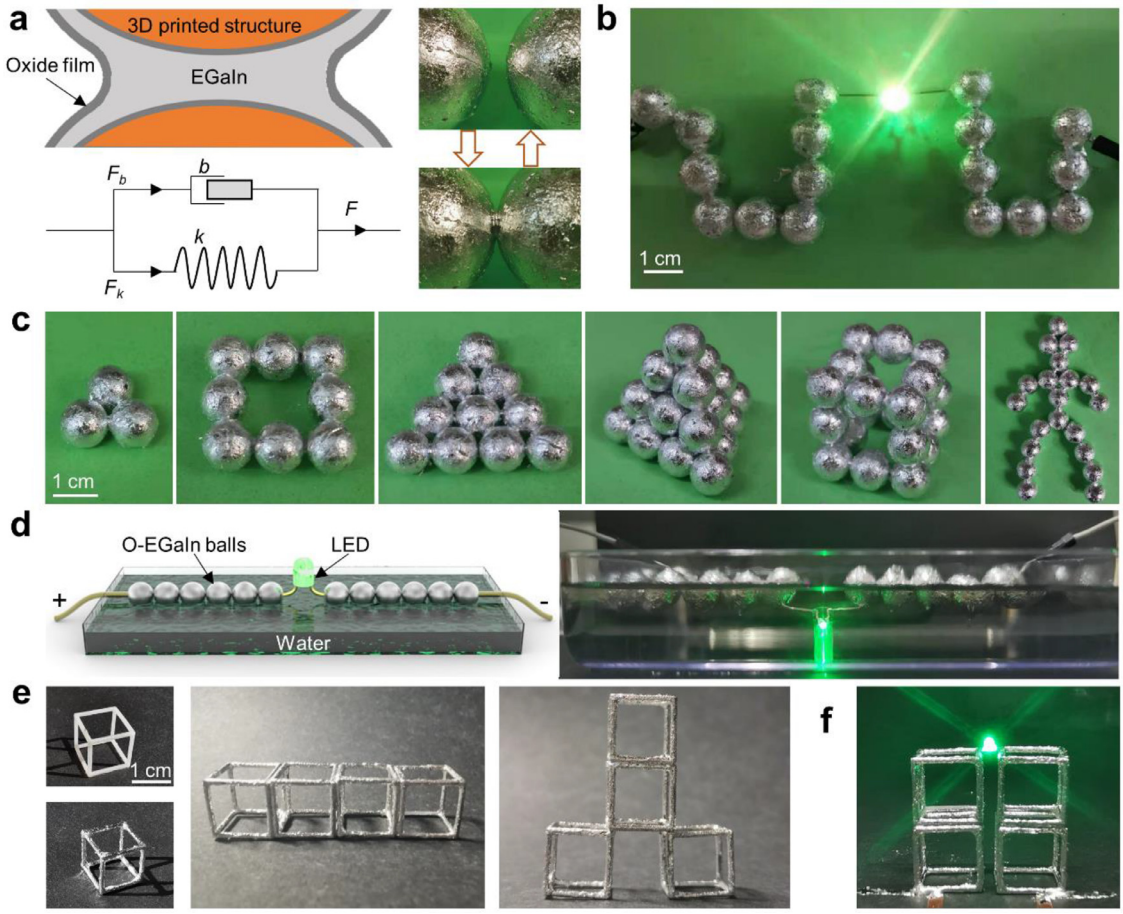

Fig. 5.. Liquid bridge of O-EGaIn coating for reconfigurable 3D electronics. (a) The schematic diagram and photos of liquid metal bridge between two balls. (b) Many liquid bridges connected balls formed a continuous conductive path to connect a LED light. (c) Complex planar and 3D structures assembled by many balls. (d) A floating 3D electronic on the water. (e) Different 3D conductive structures assembled by some SLA printed cubic frames. (f) A 3D conductive structure was assembled to connect a LED light.

covering the surface of 3D printed structure with O-EGaIn (Fig. 4f). Moreover, the mechanical properties of the O-EGaIn electronics can be regulated by changing the fabrication method or materials of the 3D structures, resulting in 3D sensors sensitive to strain. A stretchable 3D mesh structure was fabricated using Ecoflex on which the O-EGaIn could adhere directly. Figure S9 shows the fabrication method of the stretchable 3D mesh structure. Thanks to the excellent stretchability of Ecoflex, the 3D mesh electronic could be stretched to 200% strain and maintain good electrical stability. Fig. 4g depicted the relative resistance curve of the 3D mesh electronic under various strains, which exhibited an excellent linear relationship between the strains and its relative resistance.

The semiliquid state of O-EGaIn coating could form liquid bridges with the adjacent coating, resulting in assembly of more complex 3D sturcntures. To study the mechanical properties of liquid bridges, polyethylene foam balls (diameter of 1 cm) were selected as the 3D substrates, which were covered with PMA and O-EGaIn coating sequentially. A liquid bridge similar as the welding effect between two metals [39] could be formed between two neighboring balls (Fig. 5a). The schematic diagram shows a simplified mechanical model of the liquid metal bridge, which can be equivalent to a damper and a spring connected parallely. The damper is formed by the viscous oxide film composed of EGaIn oxides, while the spring is formed by the elastic core composed of EGaIn. The liquid bridge model can then be represented by a Kelvin-Voigt viscoelastic model, which was composed of elastic part (F_k) and damping part (F_b). Thus, the liquid bridge force (F) could be calculated according to Equation 2.

$$F = F_k + F_b = -kx - bx \quad (2)$$

where, x is the stretching length of liquid bridge; k is the elastic constants; b is the viscosity constants. Here, k and b increase with the increase of the contact area between two balls. Therefore, the adhesion of liquid bridge increased with the increase of ball diameter. These liquid bridges could weld the metal coating on the balls surface and form a continuous conductive path, which could be used to connect electronic components, as shown in Fig. 5b. More importantly, the conductive path was reconfigurable, which could be adjusted according to the distribution of electronic components. These balls could be connected into complex planar structures by liquid bridges, and even form 3D structures with the help of liquid bridge adhesion (Fig. 5c). Besides, this method could also easily print O-EGaIn on larger diameter balls to build larger 3D electronics (Figure S10). Thanks to the low density characteristics of polyethylene foam, these balls covered with O-EGaIn could be assembled into a floating 3D electronic on the water. Fig. 5d shows that a series of O-EGaIn balls are connected into wires through the liquid bridges to light a LED light on the water surface. Therefore, it was easy to build more complex 3D electronic through the stacking and arrangement of simple 3D printed structures. There were some SLA printed cubic frames completely covered with O-EGaIn coating, which could form liquid bridges with adjacent cubic frames and built into different 3D conductive structures, as shown in Fig. 5e. The 3D conductive structures could be

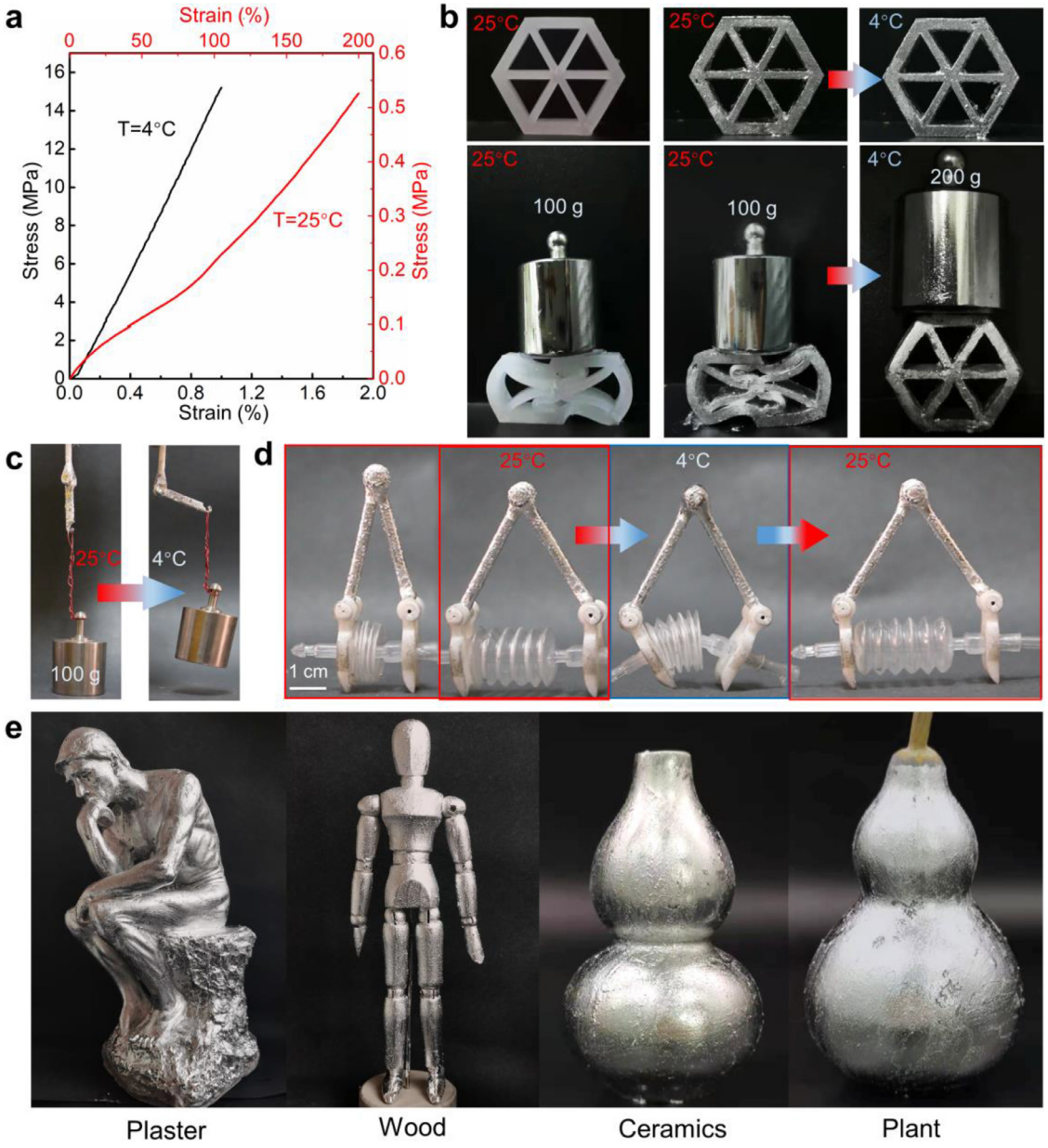

Fig. 6.. Characterization and application of solid liquid transition of O-EGaIn coating. (a) Stress–strain curves of O-EGaIn coating at 25 and 4 °C. (b) Demonstration of the stiffness variation of a hexagonal structure with O-EGaIn coating. (c) Demonstration of the stiffness variation of a SLA printed connecting rod structure covered with O-EGaIn coating. (d) Demonstration of the application of a crawling robot using pneumatically actuator and connecting rod structure, where the O-EGaIn coating acted as a variable stiffness exoskeleton. (e) The universality of this method to fabricate 3D electronics on various common items in life.

served as functional electronics by combining with electronic components, as shown in Fig. 5f. Above all, with the benefit of welding effect of liquid bridges, the assembled 3D electronics could adjust their structure in real time, which provided a new direction for the study of reconfigurable 3D electronics and even 4D electronics (Automatic mechanical devices enabled change in assembly mode over time).

In addition, the O-EGaIn with low melting temperature had a significant difference in elastic modulus between solid and liquid states (Young's modulus of solid gallium was 9.8 GPa [42]). Here, we used a silicone elastomer (Ecoflex) film with elastic modulus of 125 kPa as the substrate material (3 cm x 1 cm x 1 mm), which was covered with O-EGaIn coating. To investigate the thermomechanical behavior of the O-EGaIn coated 3D structures, we performed a dynamic mechanical analysis test. Fig. 6a shows that the elastic modulus is remarkably higher (1.5 GPa) at low temperatures (4 °C) than that (0.21 MPa) at room temperature due to the melting of O-EGaIn coating. We further examined the stiffness variation of the thermally activated O-EGaIn coating by pressing a 100 g weight onto a hexagonal structure before and after printing O-EGaIn coating at room temperature, and pressing a 200 g weight onto a hexagonal structure with O-EGaIn coating at 4 °C (Fig. 6b). The results in Fig. 6b showed that the O-EGaIn coating could support 200 g weight with nearly invisible deformation at low temperature, while it became soft with significant deformation under the pressure of 100 g weight at room temperature. Besides, the solid-liquid phase transition of O-EGaIn coating could be served as skeletal networks for the joint control of rigid robots. For example, a SLA printed bendable structure with a joint covered with O-EGaIn coating was used to lift a 100 g weight at 25 and 4 °C (Fig. 6c). It could be seen that the solidified O-EGaIn coating limited the joint movement to balance the 100 g weight at 4 °C. Fur-

thermore, we demonstrated a crawling robot using pneumatically actuator and the bendable structure. Inflation and extraction of the balloon could adjust the included angle of the joint of the bendable structure, where the covered O-EGaIn coating acted as a variable stiffness exoskeleton. Fig. 6d and Video S5 show that the joint is relaxed, and the robot moves forward; then the exoskeleton is frozen in this position while the balloon is inflated, and the robot is locked; later the exoskeleton is heated and the joint is relaxed again.

One attractive feature of the O-EGaIn printing approach is the capability to adapt to many commonly rough materials. With the assistance of PMA coating, it is possible to print liquid metal on many common items in daily life as shown in Fig. 6e and Video S6. Figure S11 shows the common items before and after printing PMA coating.

Finally, an experiment was carried out to show the printability of O-EGaIn and PMA glue. PMA glue has good fluidity and can be directly injected into the needle tube. Because there are many solid metal oxides in O-EGaIn, it is difficult to print with the needle used in direct ink writing. Thus, the O-EGaIn was adhered to the brush, and the brush is used to adhere the O-EGaIn to the substrate surface. As shown in Figure S12, the PMA glue was directly printed on a complex 3D curved surface using a needle tube (0.2 mm diameter), then the O-EGaIn was adhered to the PMA glue surface using a brush.

4. Conclusion

In summary, we had reported a 3D electronics fabrication scheme based on spatially selective adhesion mechanism of O-EGaIn between 3D substrate materials and PMA coating. Through scraping metal oxides from the surface of EGaIn, we developed O-EGaIn material with low liquidity that was more suitable as conductive coating. We revealed the principle of selective adhesion, which depended on substrate surface roughness and interfacial chemical interaction. We demonstrated the applicabilities of the approach by using it to fabricate complex conductive structures on various 3D printed materials via several common 3D printing methods. Besides, this technique could be applied to develop reconfigurable 3D electronics and reversible stiffness robots based on the phase transition and contact welding of O-EGaIn coating. It can be realized that such method was not only limited to fabricate electronics on 3D printed materials. Here, polyethylene foam, stretchable silicone and even common items in daily life (gypsum, ceramics, wood and plant) were also served as the 3D substrate materials, which showed multiple mechanical properties for stretchable and lightweight electronics. Meanwhile, some limitations pointed out the direction for the further development of the present technology. For example, the printing precision of common 3D printing methods currently available was about 200 μm. Along this direction, one could develop micro 3D electronics via microstereolithography (PμSL) 3D printing in the new future. Overall, the fast fabrication of liquid metal based 3D electronics opened new opportunities to build 3D functional devices for the coming society.

5. Author contributions

J.L. and R.G. designed the study, analyzed the results, and wrote the manuscript. R.G. and Z.Y. performed the experiments. X.H. wrote the manuscript.

Declaration of Competing Interest

The authors declare no competing interests.

Acknowledgements

This work was financially supported by National Nature Science Foundation of China under Key Project No. 51890893 and 91748206.

Supplementary materials

Supplementary material associated with this article can be found, in the online version, at doi:10.1016/j.apmt.2021.101236.

Reference

[1] Y.A. Huang, W. Hao, X. Lin, Y. Duan, Z. Hui, B. Jing, Y. Dong, Z. Yin, Mater. Horiz 6 (2019) 642–683, doi:10.1039/C8MH01450G.
[2] E. Macdonald, R. Wicker, Science 353 (2016) aaf2093-aaf2093, doi:10.1126/science.aaf2093.
[3] T.J. Wallin, J. Pikul, R.F. Shepherd, Nat. Rev. Mater. 3 (2018) 84–100, doi:10.1038/s41578-018-0002-2.
[4] Z. Zhu, S.Z. Guo, H. Tessa, E. Cindy, X. Fan, T. Jakub, M.C. Mcalpine, Adv. Mater. 30 (2018) 1707495, doi:10.1002/adma.201870165.
[5] Z. Xuan, J. Yao, B. Liu, J. Yan, L.U. Lei, L. Yi, H. Gao, X. Li, Nano Lett 18 (2018) 4247–4256, doi:10.1021/acs.nanolett.8b01241.
[6] D. Kokkinis, M. Schaffner, A.R. Studart, Nat. Commun. 6 (2015) 8643, doi:10.1038/ncomms9643.
[7] M. Zhang, M. Zhao, M. Jian, C. Wang, A. Yu, Z. Yin, X. Liang, H. Wang, K. Xia, X. Liang, Matter 1 (2019) 168–179, doi:10.1016/j.matt.2019.02.003.
[8] J.J. Adams, E.B. Duoss, T.F. Malkowski, M.J. Motala, B.Y. Ahn, R.G. Nuzzo, J.T. Bernhard, J.A. Lewis, Adv. Mater. 23 (2011) 1335–1340, doi:10.1002/adma.201003734.
[9] A. Radke, T. Gissibl, T. Klotzbücher, P.V. Braun, H. Giessen, Adv. Mater. 23 (2011) 3018–3021, doi:10.1002/adma.201100543.
[10] R. Hensleigh, H. Cui, Z. Xu, J. Massman, D. Yao, J. Berrigan, X. Zheng, Nat. Electron. 3 (2020) 216–224, doi:10.1038/s41928-020-0391-2.
[11] G. Saada, M. Layani, A. Chernevousky, S. Magdassi, Adv. Mater. Technol. 2 (2017) 1600289, doi:10.1002/admt.201770020.
[12] H. Luo, C. Wang, C. Linghu, K. Yu, C. Wang, J. Song, Natl. Sci. Rev. 7 (2020) 296–304 https://academic.oup.com/nsr/article/7/2/296/5544002.
[13] S. Kim, J. Wu, A. Carlson, S.H. Jin, A. Kovalsky, P. Glass, Z. Liu, N. Ahmed, S.L. Elgan, W. Chen, P.M. Ferreira, M. Sitti, Y. Huang, J.A. Rogers, Proc. Natl. Acad. Sci. U.S.A. 107 (2010) 17095–17100 https://www.pnas.org/content/107/40/17095.
[14] C. Yang, H. Zhang, Y. Liu, X.Wei Z.Yu, Y. Hu, Adv. Sci. 5 (2018) 1801070, doi:10.1002/advs.201801070.
[15] Z. Yan, F. Zhang, F. Liu, M. Han, D. Ou, Y. Liu, Q. Lin, X. Guo, H. Fu, Z. Xie, Sci. Adv. 2 (2016) e1601014, doi:10.1126/sciadv.1601014.
[16] P. Li, Y. Zhang, Z. Zheng, Adv. Mater. 31 (2019) 1902987, doi:10.1002/adma.201902987.
[17] Y. Jeong, J. Kim, Z. Xie, Y. Xue, S. Won, G. Lee, S. Jin, S. Hong, X. Feng, Y. Huang, NPG Asia Mater 9 (2017) e443, doi:10.1038/am.2017.189.
[18] E.J. Markvicka, M.D. Bartlett, X. Huang, C. Majidi, Nature Mater 17 (2018) 618–624, doi:10.1038/s41563-018-0084-7.
[19] M. Varga, A. Mehmann, J. Marjanovic, J. Reber, C. Vogt, K.P. Pruessmann, G. Tröster, Adv. Mater. 29 (2017) 1703744.1-1703744.7, doi:10.1002/adma.201703744.
[20] S. Cheng, C. Hang, L. Ding, W. Zheng, X. Jiang, Matter 3 (2020) 1–21, doi:10.1016/j.matt.2020.08.029.
[21] W. Zhang, J. Chen, X. Li, Y. Lu, Small 16 (2020) 2004190, doi:10.1002/smll.202004190.
[22] S.Y. Wu, C. Yang, W. Hsu, L. Lin, Microsyst. Nanoeng. 1 (2015) 15013, doi:10.1038/micronano.2015.13.
[23] J. Xie, X. You, Y. Huang, Z. Ni, Z. Chen, Nat. Commun. 11 (2020) 5793, doi:10.1038/s41467-020-19711-y.
[24] L. Zhou, Q. Gao, J. Zhan, C. Xie, J. Fu, ACS Appl. Mater. Interfaces 10 (2018) 23208–23217, doi:10.1021/acsami.8b06903.
[25] Y. He, L. Zhou, J. Zhan, Q. Gao, J. Fu, C. Xie, H. Zhao, Y. Liu, 3D Print Addit. Manuf. 5 (2018) 195–203, doi:10.1089/3dp.2017.0147.
[26] Y. Zheng, Z. He, Y. Gao, J. Liu, Sci. Rep. 3 (2013) 1786, doi:10.1038/srep01786.
[27] Y. Yu, F. Liu, R. Zhang, J. Liu, Adv. Mater. Technol. 2 (2017) 1700173, doi:10.1002/admt.201770050.
[28] C. Ladd, J. So, J. Muth, M. Dickey, Adv. Mater. 25 (2013) 5081–5085, doi:10.1002/adma.201370225.
[29] Q. Zhang, Y. Zheng, J. Liu, Frontiers in Energy 6 (2012) 311–340, doi:10.1007/s11708-012-0214-x.
[30] J.W. Boley, E.L. White, G.T. Chiu, R.K. Kramer, Adv. Funct. Mater. 24 (2014) 3501–3507, doi:10.1002/adfm.201303220.
[31] Y.G. Park, H.S. An, J.Y. Kim, J.U. Park, Sci. Adv 5 (2019) eaaw2844, doi:10.1126/sciadv.aaw2844.
[32] M. Tavakoli, M.H. Malakooti, H. Paisana, Y. Ohm, D.G. Marques, P.A. Lopes, A.P. Piedade, A.T. Almeida, C. Majidi, Adv. Mater. 30 (2018) 1801852, doi:10.1002/adma.201801852.
[33] S. Zhang, B. Wang, J. Jiang, K. Wu, C. Guo, Z. Wu, ACS Appl. Mater. Interfaces 11 (2019) 7148–7156, doi:10.1021/acsami.8b20595.

[34] I.V. Meerbeek, B.M. Murray, J. Kim, S. Robinson, P. Zou, M. Silberstein, R. Shepherd, Adv. Mater. 28 (2016) 2801–2806, doi:10.1002/adma.201505991.
[35] X. Wang, X. Liu, P. Bi, Y. Zhang, Y. Fan, ACS Appl. Mater. Interfaces 12 (2020) 53966–53972 https://dx.doi.org/10.1021/acsami.0c16438.
[36] Y. Hao, T. Wang, Z. Xie, W. Sun, Z. Liu, X. Fang, M. Yang, L. Wen, J. Micromech, Microeng. 28 (2017) 024004, doi:10.1088/1361-6439/aa9d0e.
[37] F. Deng, Q.K. Nguyen, P. Zhang, Addit. Manuf. 33 (2020) 101117, doi:10.1016/j.addma.2020.101117.
[38] X. Wang, L. Fan, J. Zhang, X. Sun, H. Chang, B. Yuan, R. Guo, M. Duan, J. Liu, Adv. Funct. Mater. 29 (2019) 1907063, doi:10.1002/adfm.201907063.
[39] R. Guo, S. Yao, X. Sun, J. Liu, Sci. China Mater. 62 (2019) 982–994, doi:10.1007/s40843-018-9400-2.
[40] R. Guo, J. Tang, S. Dong, J. Lin, H. Wang, J. Liu, W. Rao, Adv. Mater. Technol. 3 (2018) 1800265, doi:10.1002/admt.201800265.
[41] B. Yuan, C. Zhao, X. Sun, J. Liu, Adv. Funct. Mater. 30 (2020) 1910709, doi:10.1002/adfm.201910709.
[42] B. Yuan, C. Zhao, X. Sun, J. Liu, Adv. Eng. Mater. 21 (2019) 1900530, doi:10.1002/adem.201900530.